The Astrophysical Journal, 817:138 (5pp), 2016 February 1 doi:10.3847/0004-637X/817/2/138


# HIGH PRECISION ROVIBRATIONAL SPECTROSCOPY OF $OH^+$

Charles R. Markus[1], James N. Hodges[1], Adam J. Perry[1], G. Stephen Kocheril[1], Holger S. P. Müller[2], and Benjamin J. McCall[1,3]
[1] Department of Chemistry, University of Illinois, Urbana, IL 61801, USA; bjmccall@illinois.edu
[2] I. Physikalisches Institut, Universität zu Köln, Zülpicher Str. 77, D-50937 Köln, Germany
[3] Department of Astronomy, University of Illinois, Urbana, IL 61801, USA
*Received 2015 November 5; accepted 2015 December 18; published 2016 January 27*

## ABSTRACT

The molecular ion $OH^+$ has long been known to be an important component of the interstellar medium. Its relative abundance can be used to indirectly measure cosmic ray ionization rates of hydrogen, and it is the first intermediate in the interstellar formation of water. To date, only a limited number of pure rotational transitions have been observed in the laboratory making it necessary to indirectly calculate rotational levels from high-precision rovibrational spectroscopy. We have remeasured 30 transitions in the fundamental band with MHz-level precision, in order to enable the prediction of a THz spectrum of $OH^+$. The ions were produced in a water cooled discharge of $O_2$, $H_2$, and He, and the rovibrational transitions were measured with the technique Noise Immune Cavity Enhanced Optical Heterodyne Velocity Modulation Spectroscopy. These values have been included in a global fit of field free data to a $^3\Sigma^-$ linear molecule effective Hamiltonian to determine improved spectroscopic parameters which were used to predict the pure rotational transition frequencies.

*Key words:* astrochemistry – ISM: molecules – methods: laboratory: atomic – submillimeter: ISM

## 1. INTRODUCTION

Molecular ions play a central role in the chemistry of the interstellar medium. Their reactivity with neutral species overshadows other chemical processes in the cold and diffuse environments of molecular clouds. One important example is $OH^+$, which is involved in a number of astrochemical processes. Its formation in diffuse clouds is initiated by cosmic ray ionization of atomic hydrogen into $H^+$, which can undergo an endothermic charge transfer with atomic oxygen to form $O^+$. Hydrogen abstraction with $H_2$ then leads to the subsequent formation of $OH^+$, $H_2O^+$, and $H_3O^+$. Dissociative recombination with electrons destroys all three of these species yielding neutral OH and $H_2O$ along with other products. These competing processes allow for the relative abundances of $OH^+$, $H_2O^+$, and $H_3O^+$ to act as a probe of cosmic ray ionization rates and molecular hydrogen fractions in molecular clouds (van Dishoeck & Black 1986; Hollenbach et al. 2012; Indriolo et al. 2015).

Due to interference of telluric water, observatories were only able to detect rotational transitions of $H_3O^+$ (Wootten et al. 1991) until recently. The Heterodyne Instrument for the Far-Infrared aboard the orbiting telescope *Herschel* and high altitude ground based facilities enabled the first observations of $H_2O^+$ and $OH^+$ (Ossenkopf et al. 2010; Wyrowski et al. 2010). Near-ultraviolet absorption from $OH^+$ was detected shortly thereafter using the Very Large Telescope's Ultraviolet and Visual Echelle Spectrograph (Krełowski et al. 2010). The termination of *Herschel* has limited terahertz observations of $OH^+$ to high altitude observatories on the Atacama plateau and aboard aircraft such as the Stratospheric Observatory For Infrared Astronomy (SOFIA). Because of the low temperatures in translucent and diffuse molecular clouds, most of these measurements are of the ground state rotational transitions near 1 THz. There have also been observations of $OH^+$ by emission within our galaxy in photon-dominated regions (van der Tak et al. 2013; Aleman et al. 2014; Etxaluze et al. 2014). Highly rotationally excited transitions of $OH^+$ were detected with the moderate resolution Photodetector Array Camera and Spectrometer on board *Herschel* in absorption in the nearby galaxies Arp 220 and NGC 4418 by González-Alfonso et al. (2013) and in emission in our galaxy by Aleman et al. (2014).

The rotational structure of $OH^+$ arises from its $^3\Sigma^-$ ground electronic state. In this configuration, electron spin angular momentum $\boldsymbol{S}$ couples with the rotational angular momentum $\boldsymbol{N}$ as $\boldsymbol{J} = \boldsymbol{S} + \boldsymbol{N}$. A spin of $S = 1$ leads to the rotational levels splitting into fine structure triplets of $J = N + 1$, $N$, $N - 1$ with the exception of $N = 0$ where the only level is $J = 1$. The nuclear spin of $I = 1/2$ from the hydrogen nucleus splits each of these levels further into $F = J \pm 1/2$, where $\boldsymbol{F}$ is the total angular momentum. The strongest transitions follow the selection rule $\Delta F = \Delta J = \Delta N$. The only field free pure rotational measurements have been of the $N = 1 \leftarrow 0$ (Bekooy et al. 1985) and $N = 13 \leftarrow 12$ transitions (Liu et al. 1987). There have also been investigations with laser magnetic resonance (LMR) going as far as $N = 3 \leftarrow 2$ (Gruebele et al. 1986); though there have been cases, such as $H_2O^+$ and $CH_2$, where the field-free transition frequencies extrapolated from LMR data had errors much larger than the claimed uncertainties (Brünken et al. 2005; Ossenkopf et al. 2010). Rovibrational spectroscopy can help to improve the predictions of rotational transitions. Müller et al. (2005) combined the field free rotational data (Bekooy et al. 1985; Liu et al. 1987) with extensive infrared data by Rehfuss et al. (1992) with reported uncertainties of 0.003 $cm^{-1}$ (90 MHz) to determine an accurate set of Dunham-type spectroscopic parameters and to predict the rotational spectrum of $OH^+$ well into the terahertz region. Even at high frequencies, these predictions were accurate enough for studies with moderate resolution instruments (González-Alfonso et al. 2013; Aleman et al. 2014), but they may not be accurate enough for high resolution instruments, such as the German REceiver At Terahertz frequencies (GREAT, Heyminck et al. 2012) on board SOFIA. In the present work, we have therefore revisited the $v = 1 \leftarrow 0$ band of $OH^+$ with megahertz-level accuracy and determined improved molecular

parameters from a least squares fit to a $^3\Sigma^-$ linear molecule effective Hamiltonian. The pure rotational spectrum was predicted in turn to assist future astronomical observations with high resolution instruments at terahertz frequencies.

## 2. METHODS

The spectra were acquired with the technique Noise Immune Cavity Enhanced Optical Heterodyne Velocity Modulation Spectroscopy (NICE-OHVMS) (Siller et al. 2011). A detailed description of the instrument can be found in Hodges et al. (2013). In brief, a commercially available optical parametric oscillator (Aculight Argos 2400 SF) generates a continuous wave mid-infrared idler beam tunable from 3.2–3.9 $\mu$m with approximately 1 W of power. An electro-optic modulator applies an ~80 MHz phase modulation to the pump laser, imprinting RF sidebands onto the idler. The idler is coupled into an external cavity (finesse $\approx$ 150) which surrounds a water-cooled positive column discharge cell. The $OH^+$ ions were generated by flowing a 2:3:100 $H_2$:$O_2$:He mixture at 1.0 Torr through the cell and applying a 50 kHz sinusoidal discharge. Light transmitted through the cavity is focused onto a fast photodiode detector (Boston Electronics Vigo PVM-10.6-1x1). Two mixers referenced 90° out of phase with one another demodulate the signal from the detector at the frequency used to generate the sidebands. The velocity modulation signal is recovered by demodulating the output of each mixer at twice the driving frequency of the discharge (100 kHz) with a set of lock-in amplifiers. This improves our sensitivity by reducing residual amplitude modulation (RAM) from our electro-optic modulator and filtering out the strong signals from neutral species. The in-phase and quadrature outputs of each lock-in amplifier produce two channels for each mixer, resulting in four total channels of detection.

Frequency calibration of the idler is accomplished by taking the difference of the pump and signal frequencies which are calibrated with an optical frequency comb (Menlo Systems FC-1500; 100 MHz repetition rate). Initially, an infrared wavemeter (Bristol 621:IR-A) was used to measure the pump and signal beams and determine the integer number of comb modes between them. The difference in frequency measured by the wavemeter must be accurate to within half the repetition rate (50 MHz), otherwise a 100 MHz systematic error would occur. To ensure proper determination of the difference in comb modes, systematic offsets of the wavemeter measurements are corrected by measuring methane reference transitions in the HITRAN database (Rothman et al. 2013).

## 3. RESULTS AND ANALYSIS

Thirty lines were measured in the fundamental band with an average uncertainty of ~2.5 MHz, covering transitions $P(5)$ to $R(5)$. These results are displayed in Table 1. The frequencies reported by Rehfuss et al. (1992) are frequently lower than the remeasured values, and only three transitions are at a higher frequency.

A typical NICE-OHVMS scan can be seen in Figure 1(a). The odd lineshape is a result of the heterodyne and velocity modulation detection scheme. The sub-Doppler feature arises from the bidirectional nature of the cavity, and the line center can be extracted from this using a least squares fitting routine. Figure 1(b) is an example of a typical two channel fit with residuals. A technical description of the sub-Doppler fitting procedure can be found in Hodges et al. (2013). The feature is a blend of several Lamb dips, resulting in a sub-Doppler width of ~100 MHz. The width of each individual Lamb dip is larger than what would be expected from pressure broadening alone, and a proposed mechanism for this can be found in Mills et al. (2010). A large fringe, similar to the one seen in Figure 1, appeared in many of the spectra. The sub-Doppler fit does not appear to have been appreciably affected by the fringe since it is well reproduced within the residuals. Any random offset was further mitigated by collecting five measurements of each transition and averaging the line center frequencies. The uncertainty of each transition is reported as the standard deviation and shows an order of magnitude improvement over previous values. However, the precision of this study is not at the sub-MHz level as was achieved in other NICE-OHVMS studies (Hodges et al. 2013; Perry et al. 2014). This can be attributed to the lower signal-to-noise which is known to decrease the precision of the line centers (Hodges et al. 2013). The weak signals are likely a result of competing chemical processes such as the formation of $H_2O^+$. Gas mixtures with dilute quantities of $H_2$ can minimize this effect but still result in relatively weak signals.

**Table 1**
Present Transition Frequencies ($cm^{-1}$) of the $v = 1 \leftarrow 0$ Band of $OH^+$ with Quantum Numbers, Uncertainties Unc. ($10^{-6}$ $cm^{-1}$), and Residuals O−C ($10^{-6}$ $cm^{-1}$)

| $N'$ | $J'$ | $N''$ | $J''$ | $F' - F''$ [a] | Frequency | Unc. | O−C |
|---|---|---|---|---|---|---|---|
| 4 | 4 | 5 | 5 | ⋯ | 2778.543347 | 43 | −29.2 |
| 4 | 5 | 5 | 6 | ⋯ | 2778.752326 | 100 | −101.5 |
| 3 | 2 | 4 | 3 | 1.5−2.5, 2.5–3.5 | 2816.464225 | 55 | 151.0 |
| 3 | 3 | 4 | 4 | ⋯ | 2816.730510 | 100 | −28.3 |
| 3 | 4 | 4 | 5 | 3.5–4.5, 4.5–5.5 | 2816.948108 | 61 | 142.9 |
| 2 | 1 | 3 | 2 | 0.5–1.5, 1.5–2.5 | 2853.236859 | 25 | −36.6 |
| 2 | 2 | 3 | 3 | ⋯ | 2853.653079 | 80 | 21.6 |
| 2 | 3 | 3 | 4 | 2.5–3.5, 3.5–4.5 | 2853.889147 | 91 | −92.4 |
| 1 | 0 | 2 | 1 | 0.5–1.5 | 2887.654424 | 230 | −33.0 |
| 1 | 1 | 2 | 2 | ⋯ | 2889.261936 | 110 | 26.0 |
| 1 | 2 | 2 | 3 | 1.5–2.5, 2.5–3.5 | 2889.544385 | 46 | −22.1 |
| 1 | 1 | 2 | 1 | 0.5–1.5, 1.5–1.5 | 2891.773633 | 105 | −157.3 |
| 0 | 1 | 1 | 2 | 0.5–1.5, 1.5–2.5 | 2923.940929 | 63 | −9.9 |
| 1 | 2 | 0 | 1 | 2.5–1.5, 1.5–0.5 | 2987.324274 | 96 | 9.9 |
| 1 | 1 | 0 | 1 | 0.5–1.5, 1.5–1.5 | 2989.353127 | 63 | 111.2 |
| 2 | 3 | 1 | 2 | 3.5–2.5, 2.5–1.5 | 3017.368784 | 61 | −24.3 |
| 2 | 2 | 1 | 1 | ⋯ | 3017.612933 | 52 | 59.8 |
| 2 | 1 | 1 | 0 | 1.5–0.5 | 3019.241547 | 93 | 87.0 |
| 3 | 4 | 2 | 3 | 4.5–3.5, 3.5–2.5 | 3045.765058 | 65 | 25.1 |
| 3 | 3 | 2 | 2 | ⋯ | 3045.952199 | 69 | 63.0 |
| 3 | 2 | 2 | 1 | 2.5–1.5, 1.5–0.5 | 3046.372950 | 47 | −59.5 |
| 4 | 5 | 3 | 4 | 5.5–4.5, 4.5–3.5 | 3072.547147 | 25 | 8.2 |
| 4 | 4 | 3 | 3 | ⋯ | 3072.705383 | 39 | −45.4 |
| 4 | 3 | 3 | 2 | 3.5–2.5, 2.5–1.5 | 3072.964615 | 74 | 63.5 |
| 5 | 6 | 4 | 5 | ⋯ | 3097.691735 | 88 | 15.3 |
| 5 | 5 | 4 | 4 | ⋯ | 3097.831772 | 110 | −126.9 |
| 5 | 4 | 4 | 3 | ⋯ | 3098.033887 | 230 | 13.1 |
| 6 | 7 | 5 | 6 | ⋯ | 3121.165108 | 130 | −65.4 |
| 6 | 6 | 5 | 5 | ⋯ | 3121.292151 | 220 | −76.2 |
| 6 | 5 | 5 | 4 | ⋯ | 3121.465385 | 70 | 84.3 |

**Note.**
[a] Overlapping hyperfine structure (HFS) components (with two sets of $F$ quantum numbers) treated as intensity weighted averages. No HFS was resolved for entries without data, and transitions were treated as such.

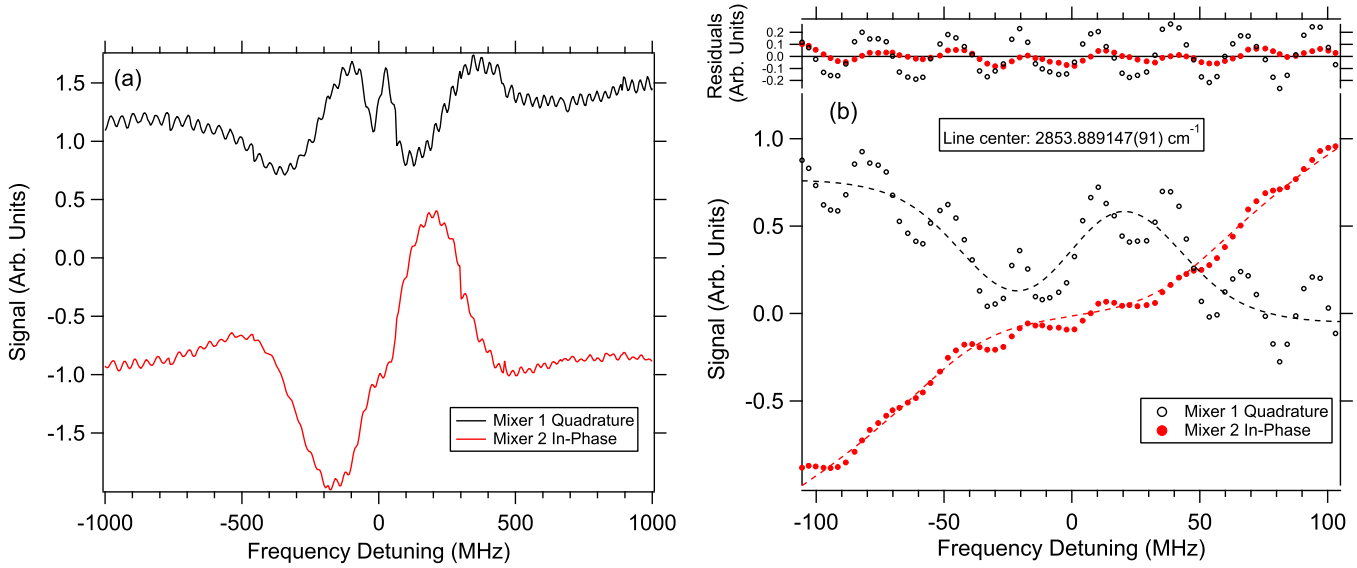


**Figure 1.** (a) A NICE-OHVMS scan of $P(3)$ $J = 3 \leftarrow 4$ centered at 2853.889147 $cm^{-1}$. The top trace is the quadrature component of the velocity modulation of the first mixer and the bottom trace is the in-phase component of the second mixer. For clarity the traces are offset from one another. (b) An enlarged comb calibrated scan of the sub-Doppler feature of $P(3)$ $J = 3 \leftarrow 4$. The colored markers represent the experimental data and the dashed lines represent the fit to the equations derived by Hodges et al. (2013). The residuals from the fit are shown above, which reproduce the fringing seen in the experimental trace.

Parameters for the $v = 0$ and $v = 1$ states were determined initially with a two-state fit of the newly measured frequencies and all data in CDMS (Müller et al. 2005) up to $v = 1$ in order to compare the compatibility of the previously reported transition frequencies and the derived spectroscopic parameters with our data. Overlapping hyperfine structure (HFS) components were treated in the fits as intensity-weighted averages, as is commonly done in fits employing the spfit/spcat program suite (Pickett 1991).

Comparing the new experimental transition frequencies with a prediction of the $v = 1 \leftarrow 0$ spectrum with $^1$H HFS revealed that a total of four of our lines should show partially resolved HFS splitting of ~0.004 $cm^{-1}$ or ~120 MHz, slightly larger than the sub-Doppler feature's width. Ultimately, trial fits and comparisons with Doppler-limited spectra established that in all four cases the frequencies determined by the Lamb dips corresponded to the stronger of the two lines with similar intensities. In all four cases the weaker line was on the side of the stronger line's Doppler profile, making precise frequency determination impossible. Hyperfine splitting turned out to be non-negligible for lower-$N$ transitions with $J = N \pm 1$ because the weak $\Delta F \neq \Delta J$ HFS components were separated from the two much stronger $\Delta F = \Delta J$ components by ~120 MHz. Because of the small uncertainties of some of our lines, these differences were important for lower-$N$ transitions. The relative intensities of these HFS components diminish rapidly with $N$, so the effects were negligible at higher $N$.

The quality of the fit was measured using the root mean square (rms) of the errors between the observed and calculated frequencies normalized to their uncertainties, which ideally should be close to 1.0. Starting with the spectroscopic parameters used by Rehfuss et al. (1992) and the HFS constants $b_F$ and $c$, it was found that the spin–spin distortion constant $\lambda_D$ was needed to achieve an rms error of 1.006. The results are shown in Table 2 with comparisons to Rehfuss et al. (1992) and Gruebele et al. (1986). The uncertainties of the rotational constant $B$, centrifugal distortion constant $D$, and the spin–spin coupling constant $\lambda$ for both $v = 0$ and $v = 1$ states were significantly improved. The constants determined by Gruebele et al. (1986) from LMR data are in strong agreement, with every parameter falling within their reported uncertainty. Nearly every parameter from Rehfuss et al. (1992) agrees with the results with the exception of the band origin $\nu_0$ which is 343 MHz higher. We have not been able to determine the cause of this discrepancy.

**Table 2**
Spectroscopic Parameters from a Two-state Fit (MHz) of $OH^+$ in Comparison to Previous Studies

| Parameter | This Work | Prev. IR[a] | Prev. LMR[b] |
|---|---|---|---|
| $B_0$ | 492346.278(146) | 492345(2) | 492346.21(69) |
| $D_0$ | 57.6166(52) | 57.614(24) | 57.544(75) |
| $H_0$ | 0.0040488(259) | 0.004062(87) | 0.0037 |
| $\lambda_0$ | 64246.00(55) | 64258(18) | 64242.9(28) |
| $\lambda_{D0}$ | −0.54(12) | ⋯ | ⋯ |
| $\gamma_0$ | −4533.85(34) | −4529.3(53) | −4534.76(124) |
| $\gamma_{D0}$ | 0.7847(153) | 0.79(15) | ⋯ |
| $b_F(^1\mathrm{H})$ | −75.14(50) | ⋯ | −71.9(125) |
| $c(^1\mathrm{H})$ | 126.01(87) | ⋯ | 130.8(202) |
| $\nu_0$ | 88629394.08(91) | 88629737(30) | ⋯ |
| $B_1$ | 470532.242(135) | 470532(2) | ⋯ |
| $D_1$ | 56.1557(44) | 56.16(2) | ⋯ |
| $H_1$ | 0.0039501(243) | 0.003969(81) | ⋯ |
| $\lambda_1$ | 63947.4(13) | 63949(15) | ⋯ |
| $\lambda_{D1}$ | −0.86(12) | ⋯ | ⋯ |
| $\gamma_1$ | −4393.34(38) | −4394.1(45) | ⋯ |
| $\gamma_{D1}$ | 0.7473(130) | 0.812(48) | ⋯ |

**Notes.**
[a] Rehfuss et al. (1992).
[b] Gruebele et al. (1986).

Subsequently, our data were combined with the complete set of previously available field-free data to determine an improved set of Dunham-type spectroscopic parameters. The parameter set used by Müller et al. (2005) for the analysis of $OH^+$ was not sufficient to reproduce the present data adequately. Trial fits

**Table 3**
Present and Previous Spectroscopic Parameters[a] of $OH^+$ in Comparison to Those of $SH^+$

| Parameter | This Work | Previous[b] | $SH^+$[c] |
|---|---|---|---|
| $Y_{10}$[d] | 3119.2892 (56) | 3119.3173 (27) | 2547.4948 (104) |
| $Y_{20}$[d] | −83.1273 (57) | −83.1606 (19) | −49.4293 (90) |
| $Y_{30}$[d] | 1.01953 (241) | 1.03525 (55) | 0.2097 (30) |
| $Y_{40} \times 10^3$[d] | 2.435 (453) | −0.795 (54) | −16.01 (34) |
| $Y_{50} \times 10^3$[d] | −0.241 (31) | … | … |
| $Y_{01}$ | 503486.90 (26) | 503486.86 (70) | 278094.99 (36) |
| $Y_{11}$ | −22435.77 (62) | −22435.87 (151) | −8577.33 (85) |
| $Y_{21}$ | 308.47 (39) | 308.28 (55) | 16.15 (32) |
| $Y_{31}$ | −1.410 (51) | −1.434 (61) | … |
| $Y_{02}$ | −58.3436 (59) | −58.3607 (128) | −14.7380 (76) |
| $Y_{12}$ | 1.4523 (37) | 1.4649 (105) | 0.1229 (27) |
| $Y_{22} \times 10^3$ | 7.51 (137) | 7.03 (192) | … |
| $Y_{03} \times 10^3$ | 4.115 (31) | 4.184 (57) | 0.46[e] |
| $Y_{13} \times 10^3$ | −0.1326 (187) | −0.1733 (288) | … |
| $\lambda_{00}$ | 64379.5 (26) | 64413.2 (38) | 171488.3 (58) |
| $\lambda_{10}$ | −254.3 (66) | −340.2 (79) | −471.8 (146) |
| $\lambda_{20}$ | −24.1 (33) | … | −79.1 (67) |
| $\lambda_{01}$ | −0.68 (11) | 0.75 (59) | −1.13 (24) |
| $\gamma_{00}$ | −4605.16 (42) | −4604.23 (108) | −5036.29 (91) |
| $\gamma_{10}$ | 143.47 (67) | 142.58 (220) | 116.4 (20) |
| $\gamma_{20}$ | −1.45 (35) | −2.14 (52) | 3.52 (64) |
| $\gamma_{01}$ | 0.796 (17) | 0.789 (36) | 0.432 (35) |
| $\gamma_{11}$ | −0.0354 (88) | … | … |
| $b_{F,00}(^1H)$ | −75.11 (49) | −74.78 (54) | −55.15 (40)[f] |
| $b_{F,10}(^1H)$ | … | … | −3.46 (79) |
| $c_{00}(^1H)$ | 125.95 (87) | 125.48 (94) | 33.60 (67) |

**Notes.** All values are in units of MHz unless otherwise stated.
[a] Numbers in parentheses are one standard deviation in units of the least significant digits.
[b] Müller et al. (2005).
[c] Müller et al. (2014).
[d] In units of $cm^{-1}$.
[e] Held fixed in Müller et al. (2014).
[f] Derived from the ground state $b_F$ and $b_{F,10}$ from Müller et al. (2014).

were performed to search among all plausible parameters for the one which reduced the rms error of the fit the most. The parameter $\lambda_{20}$, the second vibrational correction to the spin–spin coupling parameter $\lambda_{00}$, was added first. The vibrational correction $\gamma_{11}$ to the spin-rotation distortion term had a moderate effect in the overall fit, but improved the reproduction of our transition frequencies by ∼16 %. Finally, we noted that the $v = 5 \leftarrow 4$ transition frequencies from Rehfuss et al. (1992) showed very similar deviations somewhat larger than the increased uncertainties of 0.010 $cm^{-1}$. Inclusion of $Y_{50}$ in the fit not only reproduced these data much better, but also reduced the rms error of the fit considerably. Consequently, the uncertainties of this vibrational band were set to the initial 0.003 $cm^{-1}$, and the fit was rerun. The resulting spectroscopic parameters are in Table 3 together with previous values for $OH^+$ (Müller et al. 2005) as well as recent values for its heavier homolog $SH^+$ (Müller et al. 2014).

The rms error of the present fit is 0.908, hence on average the experimental transition frequencies have been reproduced within their uncertainties. The values for our data and the $v = 1 \leftarrow 0$ data of Rehfuss et al. (1992) are 1.062 and 1.107, respectively. The latter data are on average lower than the calculated frequencies by 0.0013 $cm^{-1}$ or 40 MHz, which may indicate a calibration error of approximately that magnitude.

**Table 4**
Predicted Rotational Transitions of $OH^+$ (MHz)

| $N'$–$N''$ | $J'$–$J''$ | $F'$–$F''$ | This Work | CDMS[a] |
|---|---|---|---|---|
| 1–0 | 0–1 | 1/2–1/2 | 909045.0(8) | 909045.2(10)[b] |
| 1–0 | 0–1 | 1/2–3/2 | 909159.4(8) | 909158.8(10)[b] |
| 1–0 | 2–1 | 5/2–3/2 | 971804.2(5) | 971803.8(15)[b] |
| 1–0 | 2–1 | 3/2–1/2 | 971805.3(5) | 971805.3(15)[b] |
| 1–0 | 2–1 | 3/2–3/2 | 971919.7(7) | 971919.2(10)[b] |
| 1–0 | 1–1 | 1/2–1/2 | 1032998.5(7) | 1032997.9(8) |
| 1–0 | 1–1 | 3/2–1/2 | 1033005.1(7) | 1033004.4(10)[b] |
| 1–0 | 1–1 | 1/2–3/2 | 1033112.9(7) | 1033111.8(9) |
| 1–0 | 1–1 | 3/2–3/2 | 1033119.5(7) | 1033118.6(10)[b] |
| 2–1 | 1–1 | 1/2–3/2 | 1892111.1(9) | 1892106.5(20) |
| 2–1 | 1–1 | 1/2–1/2 | 1892117.7(9) | 1892113.2(19) |
| 2–1 | 1–1 | 3/2–3/2 | 1892232.1(8) | 1892227.1(19) |
| 2–1 | 1–1 | 3/2–1/2 | 1892238.7(8) | 1892233.7(19) |
| 2–1 | 3–2 | 7/2–5/2 | 1959561.6(6) | 1959560.0(13) |
| 2–1 | 3–2 | 5/2–3/2 | 1959562.0(6) | 1959560.4(13) |
| 2–1 | 2–1 | 3/2–3/2 | 1967533.1(6) | 1967535.9(19) |
| 2–1 | 2–1 | 5/2–3/2 | 1967536.7(6) | 1967539.6(19) |
| 2–1 | 2–1 | 3/2–1/2 | 1967539.7(6) | 1967542.6(19) |
| 2–1 | 1–0 | 1/2–1/2 | 2016071.1(8) | 2016066.1(20) |
| 2–1 | 1–0 | 3/2–1/2 | 2016192.2(7) | 2016186.6(19) |
| 2–1 | 2–2 | 3/2–3/2 | 2028732.9(10) | 2028735.2(20) |
| 2–1 | 2–2 | 5/2–5/2 | 2028852.0(11) | 2028853.9(20) |
| 3–2 | 2–2 | 3/2–3/2 | 2885078.7(13) | 2885065.0(51) |
| 3–2 | 2–2 | 5/2–5/2 | 2885194.2(13) | 2885179.9(51) |
| 3–2 | 4–3 | 9/2–7/2 | 2941432.3(6) | 2941428.8(21) |
| 3–2 | 4–3 | 7/2–5/2 | 2941432.5(6) | 2941429.0(21) |
| 3–2 | 4–3 | 7/2–7/2 | 2941548.4(8) | 2941544.5(20) |
| 3–2 | 3–2 | 5/2–5/2 | 2947851.2(6) | 2947854.9(28) |
| 3–2 | 3–2 | 7/2–5/2 | 2947853.8(6) | 2947857.5(28) |
| 3–2 | 3–2 | 5/2–3/2 | 2947854.9(6) | 2947858.6(28) |
| 3–2 | 2–1 | 3/2–3/2 | 2960379.6(10) | 2960373.8(25) |
| 3–2 | 2–1 | 5/2–3/2 | 2960498.8(6) | 2960492.5(23) |
| 3–2 | 2–1 | 3/2–1/2 | 2960500.7(6) | 2960494.4(23) |
| 3–2 | 3–3 | 5/2–5/2 | 3017025.7(15) | 3017033.4(48) |
| 3–2 | 3–3 | 7/2–7/2 | 3017144.2(16) | 3017151.3(48) |
| 4–3 | 3–3 | 7/2–7/2 | 3869337.1(22) | 3869310.2(97) |
| 4–3 | 5–4 | 11/2–9/2 | 3918330.7(8) | 3918324.8(33) |
| 4–3 | 5–4 | 9/2–7/2 | 3918330.8(8) | 3918324.9(33) |
| 4–3 | 4–3 | 9/2–7/2 | 3924036.3(7) | 3924040.2(41) |
| 4–3 | 4–3 | 7/2–5/2 | 3924036.8(7) | 3924040.8(41) |
| 4–3 | 3–2 | 7/2–5/2 | 3931996.7(9) | 3931987.8(35) |
| 4–3 | 3–2 | 5/2–3/2 | 3931997.4(9) | 3931988.4(35) |
| 4–3 | 4–4 | 9/2–9/2 | 3999748.2(22) | 3999762.7(90) |
| 5–4 | 6–5 | 13/2–11/2 | 4889412.3(13) | 4889403.4(52) |
| 5–4 | 6–5 | 11/2–9/2 | 4889412.4(13) | 4889403.5(52) |
| 5–4 | 5–4 | 11/2–9/2 | 4894719.8(9) | 4894723.3(57) |
| 5–4 | 5–4 | 9/2–7/2 | 4894720.2(9) | 4894723.7(57) |
| 5–4 | 4–3 | 9/2–7/2 | 4901121.3(15) | 4901108.8(53) |
| 5–4 | 4–3 | 7/2–5/2 | 4901121.7(15) | 4901109.2(53) |

**Notes.**
[a] Müller et al. (2005).
[b] Frequencies and uncertainties are the experimental values from Bekooy et al. (1985).

The deviations are, however, within the reported uncertainties of 0.003 $cm^{-1}$ or 90 MHz (Rehfuss et al. 1992). An *a posteriori* correction of these data will likely improve the reproduction of these data and may even be beneficial for reproducing our data.

Most of the present spectroscopic parameters of $OH^+$ are close to the previous ones. Larger changes occur for parameters which have relatively large uncertainties, e.g., $\lambda_{01}$, or by inclusion of additional higher order parameters if their values appear rather small in magnitude compared to the parameters of lower and higher order ($Y_{40}$ and $\lambda_{10}$). The $Y_{ij}$ of different isotopic species scale with $\mu^{-j-i/2}$, where $\mu$ is the reduced mass. The ratios of several spectroscopic parameters of $OH^+$ and $SH^+$ are surprisingly close to these ratios, but the magnitude of $Y_{40}$ of $SH^+$ is actually much larger than that of $OH^+$.

The ratio of $\lambda_{00}$ of related molecules such as $SH^+$ and $OH^+$ scale with the ratios of $A_{SO}$, ~2.64, which holds quite well in the present case. The slight change in $b_F$ and the larger change in $c$ are usually seen for light hydrides compared to their heavier homologs. Predictions from $N = 1 - 0$ to $N = 5 - 4$ are presented in Table 4 with comparison to predictions from the current version of the CDMS. The predicted THz transitions from this work show strong agreement with the predictions from CDMS and improve the precision by a factor of 2–5. More extended predictions will be available in the catalog section of the CDMS.

These predictions can guide new searches in regions where it is feasible that $OH^+$ is rotationally excited. The only spectrograph currently capable of observing transitions of $OH^+$ above $N = 1 - 0$ is the recently upgraded GREAT instrument aboard the airborne SOFIA which covers all of the $N = 2 - 1$ rotational transitions. Rotational emission of $OH^+$ has been observed in the Orion Bar. Calculations performed by van der Tak et al. (2013) suggest that the reason for the excitation of $OH^+$ in the Orion Bar is likely a combination of collisional excitation, radiative pumping, and formation pumping. It would be interesting to search this region for $N = 2 - 1$ emission, which would enable deeper understanding of this environment. Rotationally excited transitions of $OH^+$ were already detected at moderate resolution in nearby galaxies (González-Alfonso et al. 2013) and in our galaxy (Aleman et al. 2014).

## 4. CONCLUSIONS

We have revisited the infrared spectrum of the molecular ion $OH^+$ using the spectroscopic technique NICE-OHVMS. Each transition was measured with MHz-level uncertainty by taking advantage of the narrow sub-Doppler features provided by the NICE-OHVMS technique. These values improve a number of molecular constants by at least an order of magnitude. With these improved values, ground state rotational transitions have been predicted with lower uncertainties than previously possible. This work can be used to inform future THz observations of $OH^+$.

Financial support for this work was provided by the National Aeronautics and Space Administration through project NNX13AE62G and the National Science Foundation (PHY 14-04330). J.N.H. is grateful for support from an NSF Graduate Research Fellowship (DGE 11-44245 FLLW). G.S.K. is thankful for financial support from a Gieseking Scholarship. We would also like to thank Dr. Nick Indriolo for helpful discussions.

## REFERENCES

Aleman, I., Ueta, T., Ladjal, D., et al. 2014, A&A, 566, A79
Bekooy, J. P., Verhoeve, P., Meerts, W. L., & Dymanus, A. 1985, JChPh, 82, 3868
Brünken, S., Müller, H. S. P., Lewen, F., & Giesen, T. F. 2005, JChPh, 123, 164315
Etxaluze, M., Cernicharo, J., Goicoechea, J. R., et al. 2014, A&A, 566, A78
González-Alfonso, E., Fischer, J., Bruderer, S., et al. 2013, A&A, 550, A25
Gruebele, M. H. W., Müller, R. P., & Saykally, R. J. 1986, JChPh, 84, 2489
Heyminck, S., Graf, U. U., Güsten, R., et al. 2012, A&A, 542, L1
Hodges, J. N., Perry, A. J., Jenkins, P. A., II, Siller, B. M., & McCall, B. J. 2013, JChPh, 139, 164201
Hollenbach, D., Kaufman, M. J., Neufeld, D., Wolfire, M., & Goicoechea, J. R. 2012, ApJ, 754, 105
Indriolo, N., Neufeld, D. A., Gerin, M., et al. 2015, ApJ, 800, 40
Krełowski, J., Beletsky, Y., & Galazutdinov, G. A. 2010, ApJL, 719, L20
Liu, D.-J., Ho, W.-C., & Oka, T. 1987, JChPh, 87, 2442
Mills, A. A., Siller, B. M., & McCall, B. J. 2010, CPL, 501, 1
Müller, H. S. P., Goicoechea, J. R., Cernicharo, J., et al. 2014, A&A, 569, L5
Müller, H. S. P., Schlöder, F., Stutzki, J., & Winnewisser, G. 2005, JMoSt, 742, 215
Ossenkopf, V., Müller, H. S. P., Lis, D. C., et al. 2010, A&A, 518, L111
Perry, A. J., Hodges, J. N., Markus, C. R., Kocheril, G. S., & McCall, B. J. 2014, JChPh, 141, 101101
Pickett, H. M. 1991, JMoSp, 148, 371
Rehfuss, B. D., Jagod, M.-F., Xu, L.-W., & Oka, T. 1992, JMoSp, 151, 59
Rothman, L. S., Gordon, I. E., Babikov, Y., et al. 2013, JQSRT, 130, 4
Siller, B. M., Porambo, M. W., Mills, A. A., & McCall, B. J. 2011, OExpr, 19, 24822
van der Tak, F. F. S., Nagy, Z., Ossenkopf, V., et al. 2013, A&A, 560, A95
van Dishoeck, E. F., & Black, J. H. 1986, ApJS, 62, 109
Wootten, A., Mangum, J. G., Turner, B. E., et al. 1991, ApJL, 380, L79
Wyrowski, F., Menten, K. M., Güsten, R., & Belloche, A. 2010, A&A, 518, A26